

Surface functionalization effect on physical properties and quantum capacitance of Ca₂C MXenes



Siby Thomas ^{a,1}, Sruthi Thulaseedasan ^b, Mohsen Asle Zaeem ^{a,*}

^a Department of Mechanical Engineering, Colorado School of Mines, 1500 Illinois St., Golden, CO 80401, United States

^b Department of Physics, National Institute of Technology Karnataka (NITK), Surathkal, PO: Srinivaspuram, Mangalore 575025, India

ARTICLE INFO

Keywords:

MXenes
DFT
Mechanical properties
Electronic structure
Work function
Quantum capacitance

ABSTRACT

Effects of surface terminal groups on the structural, mechanical, and electronic properties, as well as the quantum capacitance of Ca₂CT₂ (T = F-, O-, Cl-, OH-) MXenes are studied by first-principles electronic structure computations. Ca₂(OH)₂ is determined to be the most stable structure compared with Ca₂C and Ca₂CT₂ (T = F-, Cl-) MXenes, while Ca₂CO₂ is mechanically unstable. The surface terminations have a strong influence on the work function of MXene as they can alter the Fermi level and the associated electron transfer. Analyzing the atom projected density of states shows the existence of localized electron states at and around the Fermi level, generating a high charge density close to the Fermi level and resulting in relatively high quantum capacitance. The quantum capacitance of Ca₂CCl₂ is the highest (152 μF/cm²) among the studied cases, while Ca₂C(OH)₂ has the lowest quantum capacitance. The observed variations in quantum capacitance are mainly attributed to the creation and annihilation of new electronic states and the shift of Fermi level in the studied MXenes. Also, presence of surface terminations of Ca₂C MXenes considerably changes the electrode quantum capacitance and Ca₂CCl₂ is the most promising one among the studied cases.

1. Introduction

The advancement of chemical exfoliation methods opened new avenues for the mass production of nanomaterials which are in general difficult to prepare from their bulk phases. MXenes are the latest addition of two-dimensional materials (2D) family and are obtained from the selective etching of their parent MAX phase consisting of layered transition metal carbides and nitrides. The large family of MAX phases and the derived MXenes have attracted much attention due to their unique properties suitable for numerous applications including energy storage [1,2], Li- and Na-ion batteries [3,4], and catalysis [5,6].

Depending on the type of synthesizing methods such as utilized acid (e.g., hydrofluoric- HF acid) for etching the MXene from the MAX phase for removing the A atoms, the surfaces of MXenes have different terminal groups, e.g., F, O and OH [7]. It should be noted that the removal of weakly bonded A atoms in the MAX phase is the crucial step for the synthesis of MXenes [8]. Although surface functionalization is an effective strategy to exploit the full potential of MXenes, it is not well understood which functionalization is the most stable one because the terminal groups may depend on the synthesis procedures and different

compounds [9].

To date, several reports have explained the significant impact on the physico-chemical properties of freshly prepared MXenes with surface terminations [10–12]. However, it is a well-resolved fact that the precise analysis of MXene surfaces is challenging using experimental characterization techniques, because: (i) the surface is often polluted with the presence of leftover precursors and water used for etching the MXenes, (ii) the presence of light elements such as F, O and H makes the detection and characterization more complicated, and (iii) variations in the experimental setups, conditions and quality of the components sometimes aggravate efficient analysis. For example, the X-ray photoelectron spectroscopy study of select multi-layered transition metal carbide MXenes reported that etching using HF acid generates a mixture of F, O, and OH terminations in Ti₂C, Ti₃C₂, Nb₂C and Nb₄C₃ MXenes [12]. However, first-principles calculations balance the experimental studies by providing in-depth atomistic insights into the role of surface functionalization in MXenes [13,14].

In recent years, several attempts have been made to find suitable electrode materials with increased functionality and improved properties for supercapacitor applications [15,16]. Similar to batteries,

* Corresponding author.

E-mail address: zaeem@mines.edu (M. Asle Zaeem).

¹ Department of Electrical and Computer Engineering, Technical University of Munich, Hans-Piloty-Strasse 1, 85748 Garching, Munich, Germany.

supercapacitors are one of the most promising electrochemical energy storage devices due to their potential features, such as superior power density, flexibility in operation over a wide range of temperatures, superior stability, long life cycle, and zero memory effect [17–20]. The low electrical conductivity in many nanomaterials including hexagonal boron nitride (h-BN) [21], silicon carbide (SiC) [22], and transition metal oxides and hydroxides [23,24] have led to the development of new classes of 2D materials with high stability and electronic properties suitable for supercapacitor electrodes. Graphene and its allotropes and some other 2D materials have been extensively studied as electrode materials for supercapacitors due to their high electrical conductivity and large surface area [25–27]. However, the low charge density of graphene-based supercapacitors remains the main challenge, which has prompted the search for other 2D and nanomaterials [28]. Interestingly, the successful synthesis of numerous MXenes enhanced the MXene-based research for energy storage applications due to their superior mechanical stability, good hydrophilic character, and inherently high intrinsic electronic conductivity [13,15]. Besides, the exciting electrochemical characteristics of MXenes, including high charge/discharge rates hold great promise for energy storage applications [29,30].

Among the experimentally obtained MXenes, $Ti_3C_2T_2$ ($T = F, O, OH$) is best known for electrochemical applications [31,32]. Also, the presence of a transition metal in MXene with varying oxidation states helps to improve the feasibility of charge transfer in MXenes, which offers superior electrochemical properties [33,34]. In addition to this, MXenes have demonstrated a significantly larger pseudocapacitance than other capacitive materials because of their ability to store charges by pseudocapacitive mechanisms [35]. In 2017, Xin et al. investigated the possibility of bare and functionalized niobium carbide MXenes for electrode materials of supercapacitors and predicted a high C_Q ($\sim 1000F/g$) [36]. Using first-principles analysis, Li et al. reported the electronic properties and C_Q of vacancy-defect incorporated Li doped Ti_2CO_2 MXene and found that they possess a high C_Q of $6000 \mu F/cm^2$ [37]. In 2021, Bharti et al. conducted a density functional theory (DFT) study on MXene type pure and doped Nb_2N and found that they exhibit a quite high C_Q of $1196.28 \mu F/cm^2$ at $-1 V$ [38]. Recently, Wen et al. reported the enhanced supercapacitor performance of phosphorus-doped $Ti_3C_2T_x$ MXene using a combination of DFT calculations and experimental X-ray photoelectron spectroscopy; they observed a high specific capacitance of $320F/g$ at a current density of $0.5 A/g$ [39]. In addition to chemical doping, MXene composites also showed superior performance for supercapacitor applications. For example, Li et al. reported a specific capacitance of $366F/g$ at a scan rate of $2 mV/s$ for highly conductive dodecaborate/MXene composites [40]. In addition to these reports, some other transition metal-based carbide and nitride MXenes and their hybrids have been reported for supercapacitor applications [35].

Motivated by the successful synthesis of calcium carbide compositions (monoclinic phases of Ca_2C and Ca_2C_3) by high-pressure experiments [41], we recently proposed a calcium carbide monolayer (Ca_2C -ML) MXene [42]. We studied the stability and metallic features of pristine Ca_2C -ML MXene and showed its suitability for energy storage (metal-ion battery) applications [42]. However, as mentioned before, the presence of terminal groups on the surface of MXene layers are unavoidable due to their typical synthesis by the chemical etching process, [43] and the physical properties of MXenes are known to be dependent on their surface terminations [44]. From our understanding, so far no studies have been carried out for analysing the effect of surface terminations on the structure, energetics, stability, and electronic properties of Ca_2C MXenes. Since Ca_2C without termination is suitable for battery applications, we intend to test the possibility of this material for a range of applications, including batteries, capacitance, and catalysis. As a footstep in this direction, we carry out studies of Ca_2C with different surface terminations (Ca_2CT_2 ($T = F, O, Cl, OH$)) to examine their supercapacitor electrode applications.

2. Computational method

The calculations in this paper have been carried out at zero temperature. Plane wave-based density functional theory (DFT) calculations were applied using the Vienna *Ab initio* Simulation Package (VASP) [45–47]. The exchange–correlation energy functional were approximated using projected augmented wave (PAW) [48] based on generalized gradient approximation (GGA) [49] with Perdew-Burke-Ernzerhof (PBE) functional [49,50]. A very high kinetic energy cutoff of $500 eV$ was applied for obtaining accurate results. Besides, a large enough vacuum space was taken along the out-of-plane direction of the MXene sheet (20 \AA) to prevent the interaction with periodical images. We applied a $5 \times 5 \times 1$ Monkhorst Pack [51] k-point mesh to sample the Brillouin zone to optimize geometry with a convergence criterion of $10^{-6} eV$ and $10^{-3} eV/\text{\AA}$ for the total energy and residual forces, respectively. A denser k-point grid of $18 \times 18 \times 1$ was used to accurately extract the electronic density of states $D(E)$ and atom projected density of states (PDOS). To compute the band structure, hybrid calculations were carried out using the Heyd-Scuseria-Ernzerhof (HSE06) functional [52]. The van der Waals (vdW) interactions using the DFT-D3 method [53] were also considered during the entire computation, and the broadening is controlled by applying a SIGMA value of 0.05. Further, the quantum capacitance of MXene systems was computed from the electronic density of states (DOS). For that, the variation in the electronic DOS and consequently the change in quantum capacitance were examined. To analyze the dynamic stability of the functionalized Ca_2C MXenes, the finite displacement approach has been utilized with the help of the PHONOPY code [54].

3. Results and discussions

3.1. Structural models and their stability

Ca_2C is an AB_2 prototype 2D material that belongs to the hexagonal Bravais lattice, where atom C is sandwiched between two Ca atoms, as presented in Fig. 1a. The computed lattice constant and thickness of Ca_2C without any termination is 3.89 \AA and 2.33 \AA , respectively, and this is consistent with our earlier report [42]. We also computed different bond lengths in Ca_2C , and the horizontal and vertical Ca-Ca distance and Ca-C distance are 3.89 \AA , 3.24 \AA and 2.53 \AA , respectively. Further, we extended the geometry analysis of Ca_2C with the presence of different surface terminations which form Ca_2CF_2 , Ca_2CO_2 , Ca_2CCl_2 and $Ca_2C(OH)_2$ MXenes, as shown in Fig. 1b-d. In addition, we computed the lattice constant, thickness and bond lengths of these functionalized MXenes, which are detailed in Table 1.

Further, we extended our study and analyzed the cohesive (E_{Coh}) and formation (E_{form}) energies of Ca_2C and Ca_2CT_2 ($T = F^-, O^-, Cl^-, OH^-$) MXenes using these relations: [55].

$$E_{Coh} = (E_{Ca_2CT_2} - aE_{Ca} - bE_C - cE_T)/(a + b + c) \quad (1)$$

where $E_{Ca_2CT_2}$ is the total energy of Ca_2C with terminal group atoms. E_{Ca} , E_C and E_T ($T = F^-, O^-, Cl^-, OH^-$) are respectively the total energies of free Ca, C, F, O, Cl, and H atoms, estimated by constructing a large cubic lattice with a lattice parameter of 20 \AA . For the case of Ca_2C without any terminations, the cohesive energy is calculated by $E_{Coh} = (E_{Ca_2C} - aE_{Ca} - bE_C)/(a + b)$. Similarly, the formation energy (E_{form}) of pristine and surface terminated MXenes are calculated using this relation:

$$E_{form} = [E_{Ca_2CT_2} - (xE_{Ca} + yE_C + zE_T)]/N \quad (2)$$

where E_{Ca} , E_C and E_T are respectively the bulk atom energies of Ca, C and T ($T = Ca, C, F, O, Cl$) atoms obtained from their stable geometries. The x , y and z correspond to the total number of Ca, C and T atoms in the supercell, and N denotes the total number of atoms in the MXene structure. The calculated E_{Coh} and E_{form} are listed in Table 1 and indicate

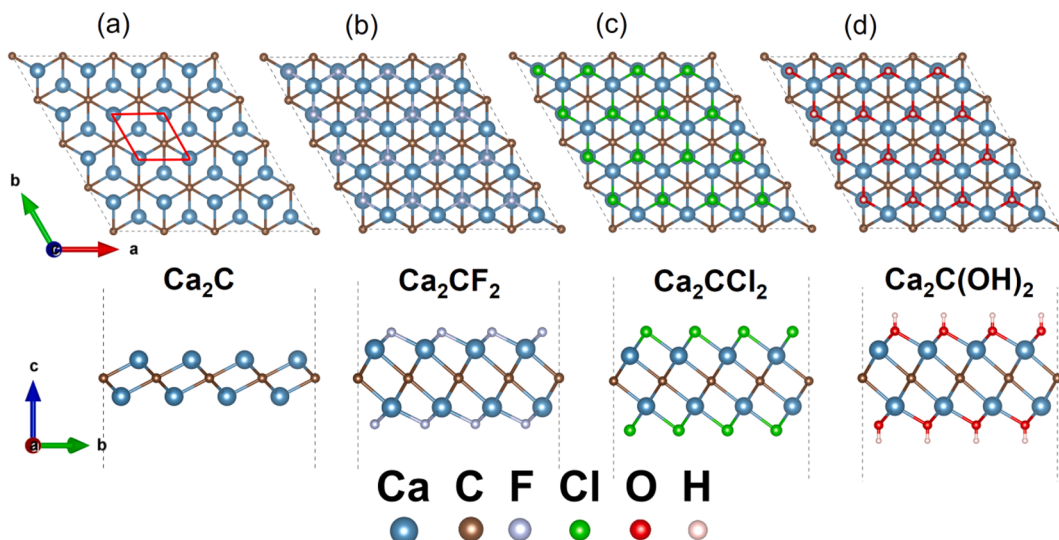


Fig. 1. The top and side geometries of (a) pristine Ca_2C MXene, (b)-(d) F^- , Cl^- , and OH^- -functionalized Ca_2C MXenes constructed using a 4×4 supercell. The unit cell is marked using a red rhombus shape as shown in (a). The structure of Ca_2CO_2 is the same as that of Ca_2CF_2 and Ca_2CCl_2 . (For interpretation of the references to color in this figure legend, the reader is referred to the web version of this article.)

Table 1

The optimized lattice constant (a), thickness (t), bond lengths (Ca-Ca along the horizontal (H) and vertical (V) directions, Ca-T ($T = \text{F}^-$, O^- , Cl^- , OH^-) and Ca-C), relative total energy/atom (ΔE), cohesive energy (E_{coh}), and formation energy (E_{form}) of the MXene structures.

MXene Structures	a (\AA)	t (\AA)	$d_{\text{Ca-Ca}}(\text{H})$ (\AA)	$d_{\text{Ca-Ca}}(\text{V})$ (\AA)	$d_{\text{Ca-C}}$ (\AA)	$d_{\text{Ca-T}}$ (\AA)	E_{Coh} (eV)	E_{form} (eV)	ΔE (eV)
Ca_2C	3.89	2.33	3.89	3.24	2.53	—	-3.88	0.43	1.26
Ca_2CF_2	3.49	5.53	3.49	4.05	2.67	2.25	-5.02	-2.41	0.08
Ca_2CO_2	3.75	4.26	3.75	4.20	2.81	2.19	-4.22	-0.81	0.08
Ca_2CCl_2	3.72	6.54	3.72	3.98	2.73	2.68	-4.11	-0.70	1.04
$\text{Ca}_2\text{C}(\text{OH})_2$	3.50	7.78	3.50	4.04	2.67	2.34	-5.16	-1.16	0.00

that cohesion among the constituent atoms of Ca_2CT_2 ($T = \text{F}^-$, O^- , Cl^- , OH^-) MXenes are stronger than atoms in Ca_2C , which suggests that the formation of Ca_2CT_2 is more feasible. Besides, we computed the relative energy stability of MXene structures and found that $\text{Ca}_2\text{C}(\text{OH})_2$ and Ca_2C possess the most and least stability, respectively. It is interesting to notice that Ca_2CT_2 ($T = \text{F}^-$, O^- , Cl^-) holds superior energy stability compared to Ca_2C , as provided in Table 1.

3.2. Mechanical and phonon stability

The mechanical stability of Ca_2C and Ca_2CT_2 ($T = \text{F}^-$, O^- , Cl^- , OH^-) MXenes are analyzed by investigating the elastic constants. Among the studied configurations, except Ca_2CO_2 , all other MXenes such as Ca_2C , Ca_2CF_2 , Ca_2CO_2 , Ca_2CCl_2 , and $\text{Ca}_2\text{C}(\text{OH})_2$ possess mechanical robustness. Besides, the stable structures satisfy the mechanical stability conditions such as $C_{11}C_{22} - C_{12}^2 > 0$ and $C_{66} > 0$. The obtained independent elastic constants (C_{11} , C_{22} , C_{12} , and C_{66}) are tabulated in Table 2. From

the elastic constants, the directional-dependent Young's modulus and Poisson's ratio are also extracted. Since Ca_2C and Ca_2CT_2 ($T = \text{F}^-$, Cl^- , OH^-) MXenes are highly isotropic, their directional-dependent elastic constants possess the same values, as shown in Table 2. Although the uniaxial elastic constants are positive for the case of Ca_2CO_2 MXenes, their shear constant becomes negative, which leads to mechanical instability. We also found that the computed elastic constants of Ca_2C MXene are comparable with our earlier research [42]. For a better comparison, we plotted the polar diagrams for Young's modulus and Poisson's ratio of mechanically stable Ca_2C and Ca_2CT_2 ($T = \text{F}^-$, Cl^- , OH^-) MXenes as shown in Fig. S1. We also noticed that the isotropic mechanical behavior of Ca_2CT_2 ($T = \text{F}^-$, Cl^- , OH^-) is associated with the circular shape of the polar diagrams.

Further, the dynamical stability of mechanically robust Ca_2C and Ca_2CT_2 ($T = \text{F}^-$, Cl^- , OH^-) MXenes are analyzed from the phonon dispersion curves. Since Ca_2CO_2 is mechanically unstable, we didn't consider it for further study. It should be noted that the local structural stability can be validated by resolving the phonon dispersion curves by demonstrating that there are no unstable or imaginary modes in the dispersion curves. It is clear from our findings (see Fig. S2) that Ca_2C is dynamically stable and is consistent with our previous study [42]. We also noticed a very miniature imaginary mode in Ca_2CCl_2 as shown in Fig. S2c. However, it is clear that Ca_2CT_2 ($T = \text{F}^-$, OH^-) structures are dynamically unstable with respect to both optical and acoustic imaginary phonon modes and should not form in principle. This is also consistent with the fact that there is no experimental evidence on the formation of Ca_2C MXenes with and without surface terminations. Although Ca_2CF_2 , Ca_2CCl_2 , and $\text{Ca}_2\text{C}(\text{OH})_2$ MXenes are characterized by small imaginary phonon modes, it may be related to the finite size of the supercells [56] as a result of the numerical truncation in the theory used for the analysis. We verified the dispersion relations of the phonon for

Table 2

Calculated independent elastic constants (C_{11} , C_{22} , C_{12} , and C_{66}), directional-dependent Young's modulus and Poisson's ratio of Ca_2C and Ca_2CT_2 ($T = \text{F}^-$, O^- , Cl^- , OH^-) MXenes.

MXene Structures	Elastic Constants (GPa)				Young's Modulus (GPa)	Poisson's Ratio
	C_{11}	C_{22}	C_{12}	C_{66}	$E_a = E_b$	$\nu_a = \nu_b$
Ca_2C	175	175	79	48	139	0.45
Ca_2CF_2	124	124	79	23	74	0.63
Ca_2CO_2	130	130	179	-25	-117	1.38
Ca_2CCl_2	55	55	35	10	33	0.63
$\text{Ca}_2\text{C}(\text{OH})_2$	89	89	54	18	57	0.60

different sizes of supercells varying from $3 \times 3 \times 1$ to $6 \times 6 \times 1$, and their main characteristics, especially imaginary frequencies, remained the same.

Since phonon spectrum is employed to assess the local stability of a system, the analysis of phonon spectrum as a function of pressure is an effective way for finding stable modes and detecting any structural transition that the 2D structure would experience with pressure [57]. Most importantly, 2D materials are frequently grown on top of a suitable substrate and the substrate may induce an effective strain on the 2D structure, and this in turn alter the dynamical stability of the 2D material [58]. Because of these reasons, the selection of substrate is also crucial for removing the imaginary frequencies in the phonon spectra [59]. Along with the role of pressure and substrate, the effects of temperature can also play a crucial role in tuning the dynamical stability of 2D materials. It is, therefore, worthwhile to consider not only the fully stable 2D structures but also those characterized by imaginary phonon modes, which are likely to be removed by temperature and/or pressure [59], and such additional analyses are out of the scope of the present work.

3.3. Electronic properties and work function analysis

We have further studied the electronic properties of Ca_2C and Ca_2CT_2 ($T = \text{F}^-, \text{Cl}^-, \text{OH}^-$) MXenes using the HSE06 functional, and the band structures are shown in Fig. 2. Similar to Ca_2C MXene,[42] we found that Ca_2CF_2 , Ca_2CCl_2 , and $\text{Ca}_2\text{C(OH)}_2$ MXenes show metallic characteristics due to the overlap of valence and conduction bands. Also, we noticed that there are electronic bands that cross the Fermi level to further confirm the metallicity. In addition, we analyzed the total and atom projected DOS of Ca_2C and Ca_2CT_2 ($T = \text{F}^-, \text{Cl}^-, \text{OH}^-$) MXenes, as shown in Fig. 3. Compared to MXenes with surface terminations, an increased DOS contribution at the Fermi level is observed for the case of Ca_2C , as shown in Fig. 3a-c. From the DOS analysis of all the structures, one can see that the states are mainly aroused from the C atoms, although the contributions from the Ca atom is also noticeable. To confirm this, the PDOS of each atom and their corresponding orbitals are analyzed, as shown in Fig. 3a-l. This also confirms the metallic behavior of Ca_2C and Ca_2CT_2 ($T = \text{F}^-, \text{Cl}^-, \text{OH}^-$) MXenes. The DOS analysis shows that the metallicity of Ca_2C , Ca_2CF_2 , Ca_2CCl_2 and $\text{Ca}_2\text{C(OH)}_2$ MXenes are mainly due to the enhanced DOS at and around the Fermi level. In the case of Ca_2C , Ca_2CF_2 , Ca_2CCl_2 and $\text{Ca}_2\text{C(OH)}_2$ MXenes, the contribution of C atoms is mainly from the px and py orbitals, and the main contribution from Ca atoms is due to the presence of d_{yz} and d_{xz} orbitals. However, from Fig. 3, the intensity and contributions of the density of states are significantly different in each case.

Further, we studied the electron localization function (ELF) of Ca_2C and Ca_2CT_2 ($T = \text{F}^-, \text{Cl}^-, \text{OH}^-$) MXenes to understand their electron

distribution and bonding features [14,60]. ELF maps of Ca_2C , Ca_2CF_2 , Ca_2CCl_2 , and $\text{Ca}_2\text{C(OH)}_2$ MXenes with a slice crossing the structural plane are shown in Fig. 4. ELF maps are renormalized at values between 1.00 and 0.00, and the values 1.0 and 0.0 indicate a state of fully localized electrons and low charge density, respectively. The normalized value of 0.5 in the ELF spectrum represents the fully delocalized electron state. The red and blue region representation in the ELF spectrum denotes highly localized and delocalized states, respectively.

In the case of all the studied MXene cases, the electrons are mostly localized around the C atom, as shown in Fig. 4. However, as compared to Ca_2CT_2 ($T = \text{F}^-, \text{Cl}^-, \text{OH}^-$), the localization is highly dominant in Ca_2C MXene, as shown in Fig. 4a. Unlike Ca_2C , ELF maps of Ca_2CF_2 , Ca_2CCl_2 , and $\text{Ca}_2\text{C(OH)}_2$ MXenes are not highly localized and are similar to the case of other MXenes such as Ti_2C and Ti_2CT_2 ($T = \text{O}^-, \text{F}^-, \text{OH}^-$) [14]. We also noticed that except Ca_2C MXene, Ca_2CT_2 ($T = \text{F}^-, \text{Cl}^-, \text{OH}^-$) MXenes show low charge density and fully delocalized electron cloud, which is evident from their ELF values between 0.50 and 0.8, as shown in Fig. 4b-d. This complete delocalization of electrons in these MXenes with surface terminations also result in a strong interconnection among atoms, which further stabilizes them. This observation also supports the general stability criterion of the studied systems, in which Ca_2CT_2 ($T = \text{F}^-, \text{Cl}^-, \text{OH}^-$) MXenes possess superior relative energy stability compared to Ca_2C , as described in section 3.1.

In addition, we calculated the work function of Ca_2C and Ca_2CT_2 ($T = \text{F}^-, \text{Cl}^-, \text{OH}^-$) MXenes. The work function (Φ) is defined as the energy difference between the Fermi energy (E_F) and the vacuum level (E_{vac}) and is represented using the relation $\Phi = E_F - E_{vac}$. Previous studies also used the same calculation method to obtain the work function of nanomaterials including MXenes,[14,21,61–63] and we used the same approach to validate the present work. The average electrostatic potential and work function of Ca_2C , Ca_2CF_2 , Ca_2CCl_2 , and $\text{Ca}_2\text{C(OH)}_2$ MXenes along the z-direction (normal to the xy plane) is shown in Fig. 5. When comparing the work function of Ca_2CT_2 ($T = \text{F}^-, \text{Cl}^-, \text{OH}^-$) MXenes with the most studied titanium carbide MXenes,[64] the Ca_2C possesses the lowest work function (1.77 eV), whereas the $\text{Ti}_2\text{C(OH)}_2$ possesses the lowest Φ (1.87 eV) among the titanium carbide cases [14]. The computed work function of Ca_2CF_2 , Ca_2CCl_2 , and $\text{Ca}_2\text{C(OH)}_2$ are 5.27 eV, 6.72 eV and 6.64 eV, respectively, as shown in Table 3. The computed work function of Ti_2C [14], Ti_2CF_2 [14] and Ti_2CCl_2 [65] are 4.53 eV, 5.14 eV and 3.97 eV, respectively. From our analysis, the surface terminations in MXene have a strong influence on the work function because of the shift of the Fermi level and associated electron transfer. Besides, the ultra-low Φ of Ca_2C is quite useful for their application in nano and optoelectronics, in comparison with Ca_2CF_2 , Ca_2CCl_2 , and $\text{Ca}_2\text{C(OH)}_2$.

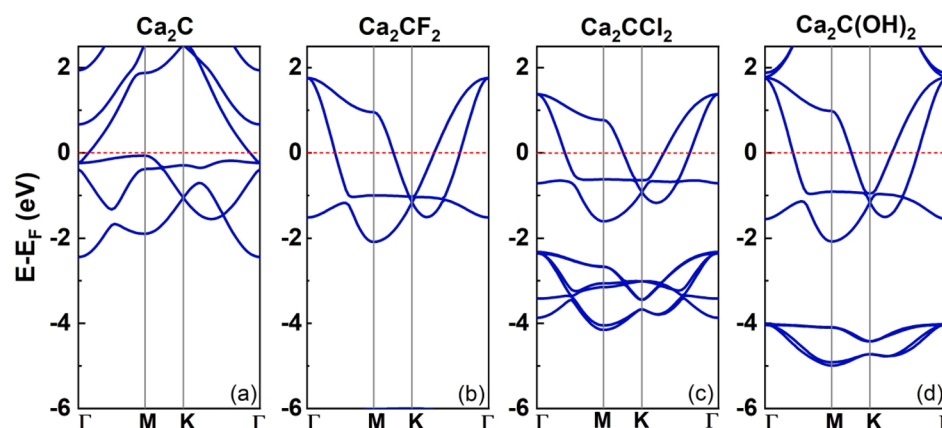


Fig. 2. Electronic band structure of (a) Ca_2C , (b) Ca_2CF_2 , (c) Ca_2CCl_2 , and (d) $\text{Ca}_2\text{C(OH)}_2$ MXenes computed using the HSE06 functional. The red dashed horizontal line stands for the Fermi level, which is fixed at 0 eV.

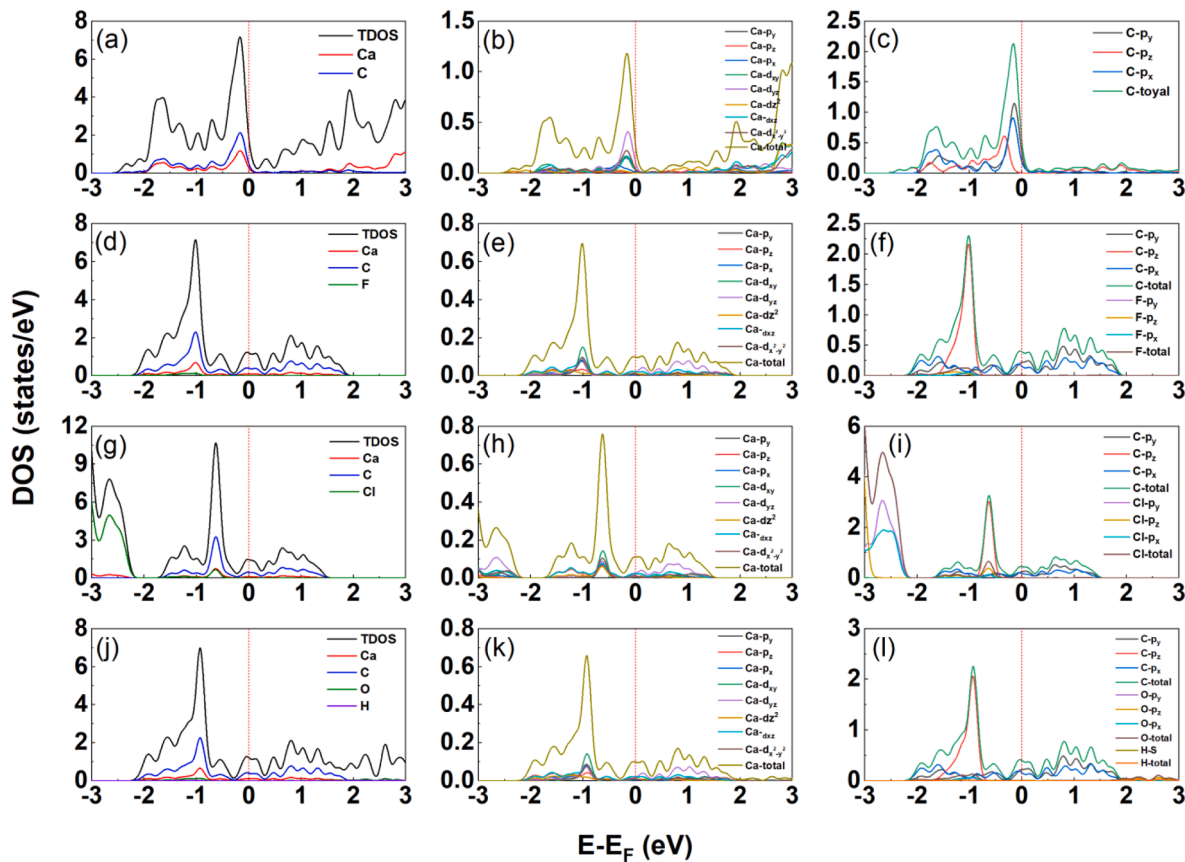


Fig. 3. The atom projected total and projected density of states (DOS) of (a)-(c) Ca₂C, (d)-(f) Ca₂CF₂, (g)-(i) Ca₂CCl₂, and (j)-(l) Ca₂C(OH)₂ MXenes. The red dashed vertical line stands for the Fermi level, which is fixed at 0 eV.

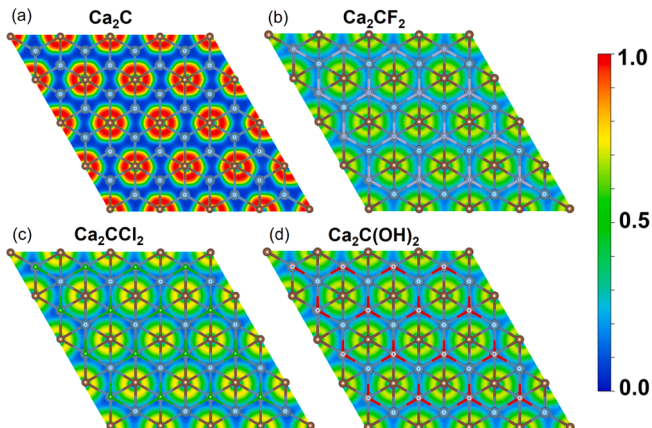


Fig. 4. ELF maps of (a) Ca₂C, (b) Ca₂CF₂, (c) Ca₂CCl₂, and (d) Ca₂C(OH)₂ MXenes with a slice crossing the structural plane. Red in the scaling bar denotes that electrons are highly localized, and blue indicates that electrons are without any localization.

3.4. Quantum capacitance and charge analysis

We studied the supercapacitor application of Ca₂CT₂ (T = F-, Cl-, OH-) MXenes by analyzing their quantum capacitance. The total capacity of the supercapacitors based on 2D materials can be considered as a series combination of the quantum capacitance (C_Q) and double layer capacitance (C_D), and this statement is valid until there is no pseudo-capacitance [66,67], and a deficit in either C_Q or C_D can affect the total capacity. In order to compute C_Q of Ca₂CT₂ (T = F-, Cl-, OH-) MXenes, we first analyzed the rate of change of excessive charges (ions) as

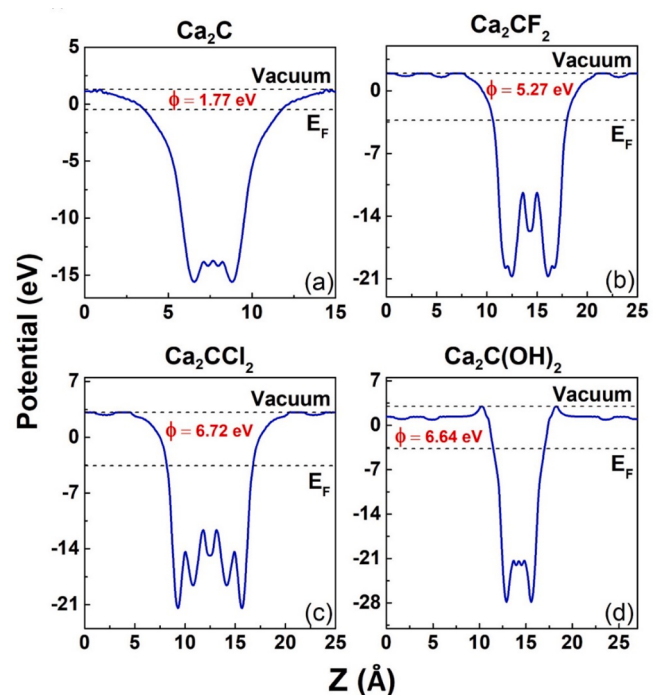


Fig. 5. Planar average electrostatic potentials and work function of (a) Ca₂C, (b) Ca₂CF₂, (c) Ca₂CCl₂, and (d) Ca₂C(OH)₂ MXenes along the z-direction (normal to the xy plane). The vacuum level (Vacuum) and Fermi energy (E_F) is also marked in the figures.

Table 3

Calculated work function (ϕ) and quantum capacitance (C_Q) of Ca_2C and Ca_2CT_2 ($T = \text{F}^-, \text{Cl}^-, \text{OH}^-$) MXenes at 300 K.

MXene Structures	$\phi(\text{eV})$	$C_Q(\mu\text{F}/\text{cm}^2)$
Ca_2C	1.77	108
Ca_2CF_2	5.27	104
Ca_2CCl_2	6.72	152
$\text{Ca}_2\text{C(OH)}_2$	6.64	100

regards the variation in applied potential [20,68]. Since the electronic energy configuration of the electrode materials is closely related to the derivative of the net charge on the substrate/electrode as far as the electrostatic potential is concerned, the C_Q is defined as:

$$C_Q = \frac{dQ}{d\phi} \quad (3)$$

where Q and ϕ are the excess charge on the electrode and chemical potential, respectively. Then, the total charge is considered as proportional to the weighted sum of the electronic DOS up to the Fermi level (E_F). However, with the presence of an applied potential, the chemical potential will also be shifted and the excess charge on the electrode (Q) can be denoted as an integral term linked with the Fermi-Dirac distribution function ($f(E)$) and the electronic DOS ($D(E)$) as.

$$Q = e \int_{-\infty}^{+\infty} D(E)[f(E) - f(E - \phi)]dE. \quad (4)$$

This implies that, if the DOS of electrode material is investigated, C_Q at any finite temperature (T) can be computed using this relation:

$$C_Q = \frac{dQ}{d\phi} = \frac{e^2}{4kT} \int_{-\infty}^{+\infty} D(E) \operatorname{Sech}^2\left(\frac{E - e\phi}{2kT}\right) dE \quad (5)$$

where e is the electronic charge and k is the Boltzmann constant. Therefore, we estimated the C_Q of Ca_2C and Ca_2CT_2 ($T = \text{F}^-, \text{Cl}^-, \text{OH}^-$) MXenes by directly analyzing the DOS. From the above expressions, the quantum capacitance (C_Q) is directly proportional to the DOS present close to the Fermi energy level. From equation (5), since $(E - e\phi)$ denotes the energy as far as the Fermi level is concerned and Sech^2 quickly drops to zero for $|x| > 0$, the density of states far away from the Fermi level does not contribute considerably to C_Q .

Since the surface termination is an important factor determining the synthesis and stability of MXenes by chemical modification, they can also effectively tune the density of states and thereby C_Q . The C_Q of Ca_2C , Ca_2CF_2 , Ca_2CCl_2 , and $\text{Ca}_2\text{C(OH)}_2$ MXenes are calculated by analyzing the DOS and found that C_Q varies with the terminal group of the MXene structure. A non-linear variation in C_Q is observed in Ca_2C and Ca_2CT_2 ($T = \text{F}^-, \text{Cl}^-, \text{OH}^-$) MXenes, as shown in Fig. 6 and Table 3. When comparing the individual, average and total DOS contributions (see Fig. 3), one can see that the variation in the intensity of DOS results in variation in capacitance. However, there exist a significant enhancement in C_Q of the studied MXenes compared to pristine graphene and MoS_2 , which has a C_Q of $\sim 1.3 \mu\text{F}/\text{cm}^2$ [20,68].

Since the conduction in Ca_2C , Ca_2CF_2 , Ca_2CCl_2 , and $\text{Ca}_2\text{C(OH)}_2$ MXenes are primarily because of the de-localized electron cloud from the p_z orbitals of C atom, the p -states are expected to exist in the vicinity of Fermi level. However, the contributions of states are significantly different in each case and a very low contribution of $\text{Ca}_2\text{C(OH)}_2$ and a very high contribution of Ca_2CCl_2 result in a small capacitance and high capacitance, respectively. The maximum value of C_Q among all studied systems is found to be $152 \mu\text{F}/\text{cm}^2$ for Ca_2CCl_2 at -0.63 eV . The variation in C_Q with respect to the energy (or electrode potential) is shown in Fig. 6. We noticed that except for Ca_2CCl_2 , all the studied MXenes show a C_Q close to each other. So, in order to check the result of surface functionalization in MXenes, the charge distribution is analyzed. The electron density contour plots associated with the studied MXenes are shown in Fig. 7. Although there exists charge inhomogeneity, it does not affect

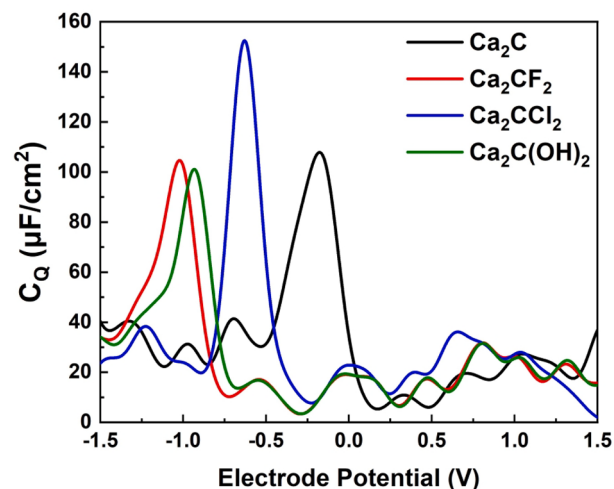


Fig. 6. The variation in quantum capacitance of Ca_2C , Ca_2CF_2 , Ca_2CCl_2 , and $\text{Ca}_2\text{C(OH)}_2$ MXenes with respect to the energy (or electrode potential).

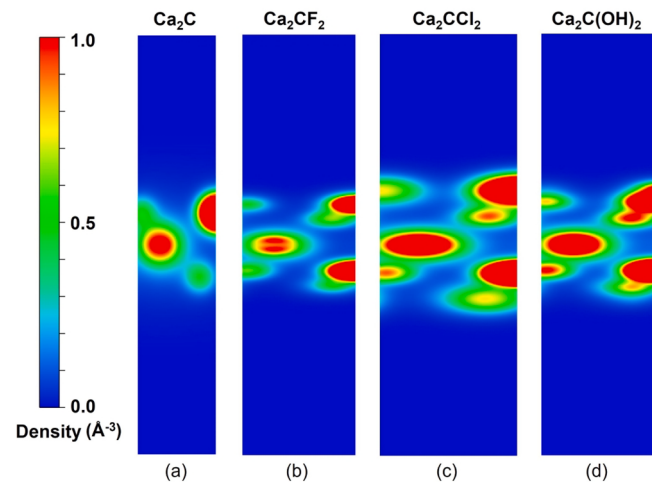


Fig. 7. Electron density Contour plots associated with (a) Ca_2C , (b) Ca_2CF_2 , (c) Ca_2CCl_2 , and (d) $\text{Ca}_2\text{C(OH)}_2$ MXenes. The relative density of the electron is specified through the color scale.

the geometry of the MXene structure. Also, the distribution and localization of charges are systematically distributed among the atoms which are directly associated with DOS, which in turn affect C_Q .

The investigated Ca_2CT_2 ($T = \text{F}^-, \text{Cl}^-, \text{OH}^-$) MXenes in this work have not been synthesized experimentally. However, a monoclinic phase of Ca_2C exists, and the accurate prediction of formation energies and stabilities of Ca_2CT_2 ($T = \text{F}^-, \text{Cl}^-, \text{OH}^-$) MXenes suggest possibility of successful synthesis of these 2D materials by experiments. Moreover, from our analyses, we noticed that Ca_2CCl_2 possesses a higher capacitance and is energetically more stable than Ca_2C , suggesting that the functionalization of Ca_2C is beneficial for some applications. Through controlling the functionalization of MXenes and possibility of addition of dopants, the present computational work may guide the fruitful synthesis of Ca_2CT_2 ($T = \text{F}^-, \text{Cl}^-, \text{OH}^-$) MXenes for different applications, including energy storage, catalysis, and sensors.

4. Summary

Through density functional theory analysis, we demonstrated the effect of surface terminations on the structure, energetics, stability, and electronic properties of Ca_2CT_2 ($T = \text{F}^-, \text{O}^-, \text{Cl}^-, \text{OH}^-$) MXenes. To reach

this observation, we first analyze the geometry, energetics and stability of Ca_2C and Ca_2CT_2 ($T = \text{F}^-, \text{O}^-, \text{Cl}^-, \text{OH}^-$) MXenes and found that the one with O-termination is mechanically unstable and is not considered for further analysis. Atom projected DOS reveals that there exist localized electron states at and around the Fermi level and are principally from the contributions of the C atom. Surface terminations in MXene have a strong impact on the work function due to the shift of Fermi level and associated electron transfer. From an application point of view, we studied the possible supercapacitor applications of Ca_2C and Ca_2CT_2 ($T = \text{F}^-, \text{Cl}^-, \text{OH}^-$) MXenes by computing the quantum capacitance. We noticed that there exist localized electron states at and around the Fermi level of these MXenes which generates a high charge density that is responsible for the high quantum capacitance. Our analysis predicted a high quantum capacitance for Ca_2CCl_2 MXene ($152 \mu\text{F}/\text{cm}^2$) compared to other studied configurations such as Ca_2C , Ca_2CCl_2 and $\text{Ca}_2\text{C}(\text{OH})_2$ ($\sim 100 \mu\text{F}/\text{cm}^2$). Functionalized Ca_2C MXenes can be promising electrode materials for supercapacitor-based devices.

CRediT authorship contribution statement

Siby Thomas: Conceptualization, Methodology, Software, Formal analysis, Validation, Writing – original draft. **Sruthi Thulaseedasan:** Methodology, Investigation, Writing – review & editing. **Mohsen Asle Zaeem:** Supervision, Conceptualization, Investigation, Resources, Writing – review & editing, Funding acquisition.

Declaration of Competing Interest

The authors declare that they have no known competing financial interests or personal relationships that could have appeared to influence the work reported in this paper.

Data availability

Data will be made available on request.

Acknowledgements

ST acknowledged the allocation of computing time by Pittsburgh Supercomputing Center (PSC) through the Bridges-2 Early User Program (EUP). ST and MAZ are thankful for the computer time granted by the Extreme Science and Engineering Discovery Environment (XSEDE) with the support of the United States National Science Foundation (NSF).

Appendix A. Supplementary data

Supplementary data to this article can be found online at <https://doi.org/10.1016/j.flatc.2022.100414>.

References

- [1] M. Ghidiu, M.R. Lukatskaya, M.-Q. Zhao, Y. Gogotsi, M.W. Barsoum, Conductive Two-Dimensional Titanium Carbide ‘Clay’ with High Volumetric Capacitance, *Nature* 516 (7529) (2014) 78–81, <https://doi.org/10.1038/nature13970>.
- [2] M.R. Lukatskaya, O. Mashatalir, C.E. Ren, Y. Dall’Agnese, P. Rozier, P.L. Taberna, M. Naguib, P. Simon, M.W. Barsoum, Y. Gogotsi, Cation Intercalation and High Volumetric Capacitance of Two-Dimensional Titanium Carbide, *Science* 341 (6153) (2013) 1502–1505.
- [3] M.-Q. Zhao, X. Xie, C.E. Ren, T. Makaryan, B. Anasori, G. Wang, Y. Gogotsi, Hollow MXene Spheres and 3D Macroporous MXene Frameworks for Na-Ion Storage, *Adv. Mater.* 29 (37) (2017) 1702410, <https://doi.org/10.1002/adma.201702410>.
- [4] M.-Q. Zhao, M. Torelli, C.E. Ren, M. Ghidiu, Z. Ling, B. Anasori, M.W. Barsoum, Y. Gogotsi, 2D Titanium Carbide and Transition Metal Oxides Hybrid Electrodes for Li-Ion Storage, *Nano Energy* 30 (2016) 603–613, <https://doi.org/10.1016/j.nanoen.2016.10.062>.
- [5] X. Wang, C. Wang, S. Ci, Y. Ma, T. Liu, L. Gao, P. Qian, C. Ji, Y. Su, Accelerating 2D MXene Catalyst Discovery for the Hydrogen Evolution Reaction by Computer-Driven Workflow and an Ensemble Learning Strategy, *J. Mater. Chem. A* 8 (44) (2020) 23488–23497, <https://doi.org/10.1039/DOTA06583H>.
- [6] Á. Morales-García, F. Calle-Vallejo, F. Illas, MXenes: New Horizons in Catalysis, *ACS Catal.* 10 (22) (2020) 13487–13503, <https://doi.org/10.1021/acscatal.0c03106>.
- [7] B. Anasori, M.R. Lukatskaya, Y. Gogotsi, 2D Metal Carbides and Nitrides (MXenes) for Energy Storage, *Nat. Rev. Mater.* 2 (2) (2017) 1–17, <https://doi.org/10.1038/natrevmats.2016.98>.
- [8] N.K. Chaudhari, H. Jin, B. Kim, D.S. Baek, S.H. Joo, K. Lee, MXene: An Emerging Two-Dimensional Material for Future Energy Conversion and Storage Applications, *J. Mater. Chem. A* 5 (47) (2017) 24564–24579, <https://doi.org/10.1039/C7TA09094C>.
- [9] R.M. Ronchi, J.T. Arantes, S.F. Santos, Synthesis, Structure, Properties and Applications of MXenes: Current Status and Perspectives, *Ceram. Int.* 45 (15) (2019) 18167–18188, <https://doi.org/10.1016/j.ceramint.2019.06.114>.
- [10] M. Mozafari, M. Soroush, Surface Functionalization of MXenes, *Mater. Adv.* 2 (22) (2021) 7277–7307, <https://doi.org/10.1039/D1MA00625H>.
- [11] R. Ibragimova, P. Erhart, P. Rinke, H.-P. Komsa, Surface Functionalization of 2D MXenes: Trends in Distribution, Composition, and Electronic Properties, *J. Phys. Chem. Lett.* 12 (9) (2021) 2377–2384, <https://doi.org/10.1021/acs.jpclett.0c03710>.
- [12] J. Halim, K.M. Cook, M. Naguib, P. Eklund, Y. Gogotsi, J. Rosen, M.W. Barsoum, X-Ray Photoelectron Spectroscopy of Select Multi-Layered Transition Metal Carbides (MXenes), *Appl. Surf. Sci.* 362 (2016) 406–417, <https://doi.org/10.1016/j.apsusc.2015.11.089>.
- [13] N. Zhang, Y. Hong, S. Yazdanparast, M. Asle Zaeem, Superior Structural, Elastic and Electronic Properties of 2D Titanium Nitride MXenes over Carbide MXenes: A Comprehensive First Principles Study, *2D Mater.* 5 (4) (2018), 045004, <https://doi.org/10.1088/2053-1583/aacbfb>.
- [14] S. Thomas, M. Asle Zaeem, Phosgene Gas Sensing of Ti_2CT_2 ($T = \text{F}^-, \text{O}^-, \text{OH}^-$) MXenes, *Adv. Theory Simul.* 4 (3) (2021) 2000250, <https://doi.org/10.1002/adts.202000250>.
- [15] K.S. Kumar, N. Choudhary, Y. Jung, J. Thomas, Recent Advances in Two-Dimensional Nanomaterials for Supercapacitor Electrode Applications, *ACS Energy Lett.* 3 (2) (2018) 482–495, <https://doi.org/10.1021/acsenergylett.7b01169>.
- [16] P. Forouzandeh, S.C. Pillai, Two-Dimensional (2D) Electrode Materials for Supercapacitors, *Mater. Today Proc.* 41 (2021) 498–505, <https://doi.org/10.1016/j.matpr.2020.05.233>.
- [17] A. Balducci, R. Dugas, P.L. Taberna, P. Simon, D. Plée, M. Mastragostino, S. Passerini, High Temperature Carbon-Carbon Supercapacitor Using Ionic Liquid as Electrolyte, *J. Power Sources* 165 (2) (2007) 922–927, <https://doi.org/10.1016/j.jpowsour.2006.12.048>.
- [18] Y. Wang, Z. Shi, Y. Huang, Y. Ma, C. Wang, M. Chen, Y. Chen, Supercapacitor Devices Based on Graphene Materials, *J. Phys. Chem. C* 113 (30) (2009) 13103–13107, <https://doi.org/10.1021/jp902214f>.
- [19] D.A.C. Brownson, D.K. Kampouris, C.E. Banks, An Overview of Graphene in Energy Production and Storage Applications, *J. Power Sources* 196 (11) (2011) 4873–4885, <https://doi.org/10.1016/j.jpowsour.2011.02.022>.
- [20] M. Mousavi-Khoshsel, E. Targholi, M.J. Momeni, First-Principles Calculation of Quantum Capacitance of Codoped Graphenes as Supercapacitor Electrodes, *J. Phys. Chem. C* 119 (47) (2015) 26290–26295, <https://doi.org/10.1021/acs.jpcc.5b07943>.
- [21] S. Thomas, M.S. Manju, K.M. Ajith, S.U. Lee, M. Asle Zaeem, Strain-Induced Work Function in h-BN and BCN Monolayers, *Phys. E Low-Dimens. Syst. Nanostructures* 123 (2020), 114180, <https://doi.org/10.1016/j.physE.2020.114180>.
- [22] M.S. Manju, S. Thomas, S.U. Lee, A. Kulangara Madam, Mechanically Robust, Self-Healing Graphene like Defective SiC: A Prospective Anode of Li-Ion Batteries, *Appl. Surf. Sci.* 541 (2021), 148417, <https://doi.org/10.1016/j.apsusc.2020.148417>.
- [23] Y. Yang, S. Niu, D. Han, T. Liu, G. Wang, Y. Li, Progress in Developing Metal Oxide Nanomaterials for Photoelectrochemical Water Splitting, *Adv. Energy Mater.* 7 (19) (2017) 1700555, <https://doi.org/10.1002/aenm.201700555>.
- [24] S.-M. Xu, H. Yan, M. Wei, Band Structure Engineering of Transition-Metal-Based Layered Double Hydroxides toward Photocatalytic Oxygen Evolution from Water: A Theoretical-Experimental Combination Study, *J. Phys. Chem. C* 121 (5) (2017) 2683–2695, <https://doi.org/10.1021/acs.jpcc.6b10159>.
- [25] M.D. Stoller, S. Park, Y. Zhu, J. An, R.S. Ruoff, Graphene-Based Ultracapacitors, *Nano Lett.* 8 (10) (2008) 3498–3502, <https://doi.org/10.1021/nl802558y>.
- [26] Q. Ke, J. Wang, Graphene-Based Materials for Supercapacitor Electrodes – A Review, *J. Materiomics* 2 (1) (2016) 37–54, <https://doi.org/10.1016/j.jmat.2016.01.001>.
- [27] Y. Chen, X. Zhang, D. Zhang, P. Yu, Y. Ma, High Performance Supercapacitors Based on Reduced Graphene Oxide in Aqueous and Ionic Liquid Electrolytes, *Carbon* 49 (2) (2011) 573–580, <https://doi.org/10.1016/j.carbon.2010.09.060>.
- [28] M.D. Stoller, C.W. Magnuson, Y. Zhu, S. Murali, J.W. Suk, R. Piner, R.S. Ruoff, Interfacial Capacitance of Single Layer Graphene, *Energy Environ. Sci.* 4 (11) (2011) 4685–4689, <https://doi.org/10.1039/C1EE02322E>.
- [29] J. Pang, R.G. Mendes, A. Bachmatiuk, L. Zhao, H.Q. Ta, T. Gemming, H. Liu, Z. Liu, M.H. Rummeli, Applications of 2D MXenes in Energy Conversion and Storage Systems, *Chem. Soc. Rev.* 48 (1) (2019) 72–133, <https://doi.org/10.1039/C8CS00324F>.
- [30] Q. Yang, Y. Wang, X. Li, H. Li, Z. Wang, Z. Tang, L. Ma, F. Mo, C. Zhi, Recent Progress of MXene-Based Nanomaterials in Flexible Energy Storage and Electronic Devices, *ENERGY Environ. Mater.* 1 (4) (2018) 183–195, <https://doi.org/10.1002/eem2.12023>.
- [31] H. Wang, J. Li, X. Kuai, L. Bu, L. Gao, X. Xiao, Y. Gogotsi, Enhanced Rate Capability of Ion-Accessible $\text{Ti}_3\text{C}_2\text{Tx}-\text{NbN}$ Hybrid Electrodes, *Adv. Energy Mater.* 10 (35) (2020) 2001411, <https://doi.org/10.1002/aenm.202001411>.

- [32] R. Cheng, T. Hu, H. Zhang, C. Wang, M. Hu, J. Yang, C. Cui, T. Guang, C. Li, C. Shi, P. Hou, X. Wang, Understanding the Lithium Storage Mechanism of Ti3C2Tx MXene, *J. Phys. Chem. C* 123 (2) (2019) 1099–1109, <https://doi.org/10.1021/acs.jpc.8b10790>.
- [33] L. Wang, M. Han, C.E. Shuck, X. Wang, Y. Gogotsi, Adjustable Electrochemical Properties of Solid-Solution MXenes, *Nano Energy* 88 (2021), 106308, <https://doi.org/10.1016/j.nanoen.2021.106308>.
- [34] F. Kong, X. He, Q. Liu, X. Qi, Y. Zheng, R. Wang, Y. Bai, Improving the Electrochemical Properties of MXene Ti3C2 Multilayer for Li-Ion Batteries by Vacuum Calcination, *Electrochimica Acta* 265 (2018) 140–150, <https://doi.org/10.1016/j.electacta.2018.01.196>.
- [35] D.D. Babu, M. Mathew, S. Thomas, in: *Fundamentals and Supercapacitor Applications of 2D Materials*, Elsevier, 2021, pp. 217–233.
- [36] Y. Xin, Y.-X. Yu, Possibility of Bare and Functionalized Niobium Carbide MXenes for Electrode Materials of Supercapacitors and Field Emitters, *Mater. Des.* 130 (2017) 512–520, <https://doi.org/10.1016/j.matdes.2017.05.052>.
- [37] X.-H. Li, S.-S. Li, X.-H. Cui, R.-Z. Zhang, H.-L. Cui, First-Principle Study of Electronic Properties and Quantum Capacitance of Lithium Adsorption on Pristine and Vacancy-Defected O-Functionalized Ti2C MXene, *Appl. Surf. Sci.* 563 (2021), 150264, <https://doi.org/10.1016/j.apsusc.2021.150264>.
- [38] Bharti, G. Ahmed, Y. Kumar, P. Boccetta, S. Sharma, Determination of Quantum Capacitance of Niobium Nitrides Nb2N and Nb4N3 for Supercapacitor Applications, *J. Compos. Sci.* 5 (3) (2021) 85, <https://doi.org/10.3390/cs5030085>.
- [39] Y. Wen, R. Li, J. Liu, Z. Wei, S. Li, L. Du, K. Zu, Z. Li, Y. Pan, H. Hu, A Temperature-Dependent Phosphorus Doping on Ti3C2Tx MXene for Enhanced Supercapacitance, *J. Colloid Interface Sci.* 604 (2021) 239–247, <https://doi.org/10.1016/j.jcis.2021.06.020>.
- [40] Z. Li, C. Ma, Y. Wen, Z. Wei, X. Xing, J. Chu, C. Yu, K. Wang, Z.-K. Wang, Highly Conductive Dodecaborate/MXene Composites for High Performance Supercapacitors, *Nano Res.* 13 (1) (2020) 196–202, <https://doi.org/10.1007/s12274-019-2597-z>.
- [41] Y.-L. Li, S.-N. Wang, A.R. Oganov, H. Gou, J.S. Smith, T.A. Strobel, Investigation of Exotic Stable Calcium Carbides Using Theory and Experiment, *Nat. Commun.* 6 (1) (2015) 6974, <https://doi.org/10.1038/ncomms7974>.
- [42] K. Rajput, V. Kumar, S. Thomas, M. Asle Zaeem, D.R. Roy, Ca2C MXene Monolayer as a Superior Anode for Metal-Ion Batteries, *2D Mater.* 8 (3) (2021), 035015, <https://doi.org/10.1088/2053-1583/abf233>.
- [43] N.M. Caffrey, Effect of Mixed Surface Terminations on the Structural and Electrochemical Properties of Two-Dimensional Ti3C2T2 and V2CT2 MXenes Multilayers, *Nanoscale* 10 (28) (2018) 13520–13530, <https://doi.org/10.1039/C8NR03221A>.
- [44] T. Schultz, N.C. Frey, K. Hantanasisirakul, S. Park, S.J. May, V.B. Shenoy, Y. Gogotsi, N. Koch, Surface Termination Dependent Work Function and Electronic Properties of Ti3C2Tx MXene, *Chem. Mater.* 31 (17) (2019) 6590–6597, <https://doi.org/10.1021/acs.chemmater.9b00414>.
- [45] G. Kresse, J. Furthmüller, Efficiency of Ab-Initio Total Energy Calculations for Metals and Semiconductors Using a Plane-Wave Basis Set, *Comput. Mater. Sci.* 6 (1) (1996) 15–50, [https://doi.org/10.1016/0927-0256\(96\)00008-0](https://doi.org/10.1016/0927-0256(96)00008-0).
- [46] G. Kresse, J. Furthmüller, Efficient Iterative Schemes for Ab Initio Total-Energy Calculations Using a Plane-Wave Basis Set, *Phys. Rev. B* 54 (16) (1996) 11169–11186, <https://doi.org/10.1103/PhysRevB.54.11169>.
- [47] P. Hohenberg, W. Kohn, Inhomogeneous Electron Gas, *Phys. Rev.* 136 (3B) (1964) B864–B871, <https://doi.org/10.1103/PhysRev.136.B864>.
- [48] P.E. Blöchl, Projector Augmented-Wave Method, *Phys. Rev. B* 50 (24) (1994) 17953–17979, <https://doi.org/10.1103/PhysRevB.50.17953>.
- [49] J.P. Perdew, K. Burke, M. Ernzerhof, Generalized Gradient Approximation Made Simple [Phys. Rev. Lett. 77, 3865 (1996)], *Phys. Rev. Lett.* 78 (7) (1997).
- [50] J.P. Perdew, J.A. Chevary, S.H. Vosko, K.A. Jackson, M.R. Pederson, D.J. Singh, C. Fiolhais, Atoms, Molecules, Solids, and Surfaces: Applications of the Generalized Gradient Approximation for Exchange and Correlation, *Phys. Rev. B* 46 (11) (1992) 6671–6687, <https://doi.org/10.1103/PhysRevB.46.6671>.
- [51] H.J. Monkhorst, J.D. Pack, Special Points for Brillouin-Zone Integrations, *Phys. Rev. B* 13 (12) (1976) 5188–5192, <https://doi.org/10.1103/PhysRevB.13.5188>.
- [52] J. Heyd, G.E. Scuseria, M. Ernzerhof, Hybrid Functionals Based on a Screened Coulomb Potential, *J. Chem. Phys.* 118 (18) (2003) 8207–8215, <https://doi.org/10.1063/1.1564060>.
- [53] S. Grimme, S. Ehrlich, L. Goerigk, Effect of the Damping Function in Dispersion Corrected Density Functional Theory, *J. Comput. Chem.* 32 (7) (2011) 1456–1465, <https://doi.org/10.1002/jcc.21759>.
- [54] A. Togo, I. Tanaka, First Principles Phonon Calculations in Materials Science, *Scr. Mater.* 108 (2015) 1–5, <https://doi.org/10.1016/j.scriptamat.2015.07.021>.
- [55] K. Kaur, D. Murali, B.R.K. Nanda, Stretchable and Dynamically Stable Promising Two-Dimensional Thermoelectric Materials: ScP and ScAs, *J. Mater. Chem. A* 7 (20) (2019) 12604–12615, <https://doi.org/10.1039/C9TA01393H>.
- [56] A. Mishra, P. Srivastava, A. Carreras, I. Tanaka, H. Mizuseki, K.-R. Lee, A.K. Singh, Atomistic Origin of Phase Stability in Oxygen-Functionalized MXene: A Comparative Study, *J. Phys. Chem. C* 121 (34) (2017) 18947–18953, <https://doi.org/10.1021/acs.jpc.7b06162>.
- [57] G.K. Pradhan, A. Kumar, S.K. Deb, U.V. Waghmare, C. Narayana, Elastic and Structural Instability of Cubic \$\{text{Sn}\}_{\{3\}}\{\text{N}\}_{\{4\}}\$ and \$\{text{C}\}_{\{3\}}\{\text{N}\}_{\{4\}}\$ under Pressure, *Phys. Rev. B* 82 (14) (2010) 144112, <https://doi.org/10.1103/PhysRevB.82.144112>.
- [58] A. Banik, T. Ghosh, R. Arora, M. Dutta, J. Pandey, S. Acharya, A. Soni, U. V. Waghmare, K. Biswas, Engineering Ferroelectric Instability to Achieve Ultralow Thermal Conductivity and High Thermoelectric Performance in Sn1-xGexTe, *Energy Environ. Sci.* 12 (2) (2019) 589–595, <https://doi.org/10.1039/C8EE03162B>.
- [59] W. Sun, Y. Li, B. Wang, X. Jiang, M.I. Katsnelson, P. Korzhavyi, O. Eriksson, I. D. Marco, A New 2D Monolayer BiXene, M2C (M = Mo, Tc, Os), *Nanoscale* 8 (34) (2016) 15753–15762, <https://doi.org/10.1039/C6NR03602C>.
- [60] A. Savin, A.D. Becke, J. Flad, R. Nesper, H. Preuss, H.G. von Schnering, A New Look at Electron Localization, *Angew. Chem. Int. Ed. Engl.* 30 (4) (1991) 409–412, <https://doi.org/10.1002/anie.199104091>.
- [61] S. Thomas, M. Asle Zaeem, A New Planar BCN Lateral Heterostructure with Outstanding Strength and Defect-Mediated Superior Semiconducting to Metallic Properties, *Phys. Chem. Chem. Phys.* 22 (38) (2020) 22066–22077, <https://doi.org/10.1039/DQCP02973D>.
- [62] S. Thomas, M. Asle Zaeem, Superior Sensing Performance of Two-Dimensional Ruthenium Carbide (2D-RuC) in Detection of NO, NO2 and NH3 Gas Molecules, *Appl. Surf. Sci.* 563 (2021), 150232, <https://doi.org/10.1016/j.apsusc.2021.150232>.
- [63] S. Thomas, V. Kumar, D.R. Roy, M. Asle Zaeem, Two-Dimensional Boron-Phosphorus Monolayer for Reversible NO2 Gas Sensing, *ACS Appl. Nano Mater.* 3 (10) (2020) 10073–10081, <https://doi.org/10.1021/acsnano.0c02072>.
- [64] M. Khazaei, M. Arai, T. Sasaki, A. Ranjbar, Y. Liang, S. Yunoki, OH-Terminated Two-Dimensional Transition Metal Carbides and Nitrides as Ultralow Work Function Materials, *Phys. Rev. B* 92 (7) (2015), 075411, <https://doi.org/10.1103/PhysRevB.92.075411>.
- [65] Y. Qin, X.-H. Zha, X. Bai, K. Luo, Q. Huang, Y. Wang, S. Du, Structural, Mechanical and Electronic Properties of Two-Dimensional Chlorine-Terminated Transition Metal Carbides and Nitrides, *J. Phys. Condens. Matter* 32 (13) (2020), 135302, <https://doi.org/10.1088/1361-648X/ab6048>.
- [66] A.J. Pak, E. Paek, G.S. Hwang, Tailoring the Performance of Graphene-Based Supercapacitors Using Topological Defects: A Theoretical Assessment, *Carbon* 68 (2014) 734–741, <https://doi.org/10.1016/j.carbon.2013.11.057>.
- [67] B.C. Wood, T. Ogitsu, M. Otani, J. Biener, First-Principles-Inspired Design Strategies for Graphene-Based Supercapacitor Electrodes, *J. Phys. Chem. C* 118 (1) (2014) 4–15, <https://doi.org/10.1021/jp4044013>.
- [68] T. Sruthi, T. Kartick, Route to Achieving Enhanced Quantum Capacitance in Functionalized Graphene Based Supercapacitor Electrodes, *J. Phys. Condens. Matter* 31 (47) (2019), 475502, <https://doi.org/10.1088/1361-648X/ab2ac0>.